J Appl Electrochem (2013) 43:847–854
DOI 10.1007/s10800-013-0570-1

ORIGINAL ARTICLE

Sn and Sb co-doped RuTi oxides supported on TiO_2 nanotubes anode for selectivity toward electrocatalytic chlorine evolution

Kun Xiong · Zihua Deng · Li Li · Siguo Chen · Meirong Xia · Li Zhang · Xueqiang Qi · Wei Ding · Shiyu Tan · Zidong Wei

Received: 3 April 2013 / Accepted: 1 June 2013 / Published online: 18 June 2013

Abstract The $(Ru_{0.3}Ti_{0.34}Sn_{0.3}Sb_{0.06})O_2$–$TiO_2$ nanotubes (TNTs) anode has been prepared via anodization, deposition, and annealing. X-ray diffraction, field-emission scanning electron microscopy, cyclic voltammetry, and linear scanning voltammetry were used to scrutinize the electrodes and the electrochemical activity. The results indicate that highly ordered TNTs with large specific surface area could be implanted with active metal oxides. The catalyst firmly binds with the TNTs and enhances the electrochemical stability of the electrode. It displays high over-potential for oxygen evolution reaction. Accordingly, the constructed $(Ru_{0.3}Ti_{0.34}Sn_{0.3}Sb_{0.06})O_2$–TNTs anode exhibits a greater potential difference (ΔE) between the evolutions of oxygen and chlorine than that exhibited by the traditional dimensionally stable anode, which is beneficial for improving the selectivity toward chlorine evolution reaction. This superior performance is explained in terms of the surface properties and geometric structure of coated catalyst, as well as the electrochemical selectivity ascribed by the addition of tin and antimony species.

Keywords TiO_2 nanotubes · RuO_2-based catalysts · Tin · Antimony · Electrocatalytic chlorine evolution

K. Xiong · Z. Deng · L. Li · S. Chen · M. Xia · L. Zhang · X. Qi · W. Ding · S. Tan · Z. Wei (✉)
State Key Laboratory of Power Transmission Equipment & System Security and New Technology, College of Chemistry and Chemical Engineering, Chongqing University, Chongqing 400044, People's Republic of China
e-mail: zdwei@cqu.edu.cn

1 Introduction

Chlorine is an essential product and widely used in the fields of chemical industry, pharmaceutical industry, and wastewater treatment. Although the electrolytic production of chlorine is a well-established industrial process, it is still necessary to further improve the efficiency of chlorine evolution reaction (CER) and long-term durability of the electrode due to the large amount of consumed electrical energy [1–3].

Currently, the most commonly used electro-catalysts in CER are so-called dimensionally stable anodes (DSA), which brought a revolution in technical electro-chemistry [4, 5]. DSA consists of a Ti substrate coated with an electrocatalytic layer containing ruthenium dioxide and titanium dioxide (RuO_2–TiO_2/Ti electrode). It exhibits excellent electrocatalytic performance toward CER [6, 7]. With density functional theory calculations, Rossmeisl et al. [8] and Hansen et al. [9] studied the mechanism of the electrochemical OER/CERs on (110) rutile surface. They have found that in OER three intermediates have to optimally bind on the electrode surface, while CER involves only a single intermediate for which an optimal bonding situation is easier to find. Accordingly, the potential necessary for CER is always smaller than the potential for OER. However, the over-potential of the electrode for CER gradually increases from 40 to 50 mV (fresh electrode) to 300 to 400 mV after long-term harsh reaction. The reason is that the catalyst coated on the Ti substrate flake off and active species dissolve at high potentials, which concomitantly result in a reduction of the number of active sites at the electrode surface [10, 11]. When the over-potential of OER is not high enough, CER is competing with OER; whereas OER facilitates the formation of a TiO_2 passive film between the Ti substrate

and the coating, resulting in the deactivation of the electrode [12]. Even though there are several strategies available to minimize the loss of Ru and the peeling of the coating [6, 13–15], the design and preparation of a novel anode with high electrocatalytic activity and stability for CER is still a challenge.

In recent years, the vertically aligned TiO_2 nanotubes (TNTs) have attracted much attention in the fields of solar energy conversion [16, 17], electrochemical energy storage [18, 19], and electro-catalysis [20, 21], because of their unique structure and high surface area as a support, which increase the effective area of the electrode and create more active sites. Pan et al. [20] reported that Ti/TiO_2NT/PbO_2 electrode possessed strong electrochemical oxidation capability and enduring stability with respect to the degradation of lignin wastewater due to its unique microstructure. Our previous studies [21] have also shown that the performance and stability of Pt/TNTs/Ti electrode for the electrochemical oxidation of methanol is remarkably enhanced. It was considered that the TNTs with large specific surface and good space utilization could improve the dispersion of the Pt nanoparticles and increase the active sites. Active metal oxides well dispersed on the TNTs are therefore expected to exhibit high electrocatalytic activity and stability for CER, albeit few reports have thus far appeared in the literature on the use of TNTs as an anodic catalyst support in CER [22].

In this work, the $(Ru_{0.3}Ti_{0.34}Sn_{0.3}Sb_{0.06})O_2$–TNTs anode was prepared via anodization, deposition, and annealing, as detailed in the next section. The obtained anode combined the advantages of the TNTs support with the coating without crack, which is favorable for improving the electrocatalytic performance and stability of the electrode. The electrodes were characterized using X-ray diffraction (XRD), field-emission scanning electron microscopy (FE-SEM), cyclic voltammetry (CV), and linear-sweep voltammetry (LSV). Electrochemical measurements were performed in a three-electrode cell system. The results were compared with that of traditional DSA.

2 Experimental

2.1 Preparation of TNTs

TiO_2 nanotubes were prepared on a Ti substrate ($60.0 \times 10.0 \times 0.5$ mm^3) using an anodization method [21]. Prior to anodization, the Ti substrate was mechanically polished with different abrasive papers and was ultrasonically cleaned in acetone, ethanol, and milli-Q water for 15 min, respectively. Afterward, the polished Ti substrate was anodized in the electrolyte of 0.5 wt% HF with a Ni foil as a counter electrode at 20 V for 40 min. The prepared TNTs with amorphous structure were washed with milli-Q water, ultrasonically cleaned for 5 min, and divided into two parts: one was annealed at 773 K for 1 h under air conditions, whereas the other amorphous TNTs were not annealed before being used as a support for depositing the metal oxides.

2.2 Preparation of the coatings

Electrodes of nominal composition $(Ru_{0.3}Ti_{0.7})O_2$ and $(Ru_{0.3}Ti_{0.34}Sn_{0.3}Sb_{0.06})O_2$ were prepared via thermal decomposition of a mixture of $RuCl_3$, $C_{16}H_{36}O_4Ti$, $SnCl_4$, and $SbCl_3$ dissolved in iso-propanol at different molar ratios. As the molar ratios of tin and antimony could obviously affect the catalytic activity and selectively of the anodes for CER, we have systematically investigated the molar ratios of tin and antimony and finally chose the optimized molar ratios with 0.3 and 0.06, respectively, for the $(Ru_{0.3}Ti_{0.34}Sn_{0.3}Sb_{0.06})O_2$. The prepared TNTs were brushed with the precursors at room temperature, followed by drying at 373 K for 10 min to allow the solvent to vaporize, and then annealed at 723 K for 10 min. This procedure was repeated ten times. Finally, the electrodes were annealed at 773 K for 1 h under ambient air. The electrode for the TNTs, subjected to an early-stage anneal pretreatment at 773 K, is denoted as $(Ru_{0.3}Ti_{0.34}Sn_{0.3}Sb_{0.06})O_2$/(773 K annealed)TNTs, and that for the TNTs without anneal preprocessing is denoted as $(Ru_{0.3}Ti_{0.34}Sn_{0.3}Sb_{0.06})O_2$–TNTs. The total Ru loading of the prepared electrode is 0.5 mg cm^{-2}. For purposes of comparison, the traditional $(Ru_{0.3}Ti_{0.7})O_2$/Ti and $(Ru_{0.3}Ti_{0.34}Sn_{0.3}Sb_{0.06})O_2$/Ti anodes were also prepared via a thermal decomposition route.

2.3 Characterization

The surface morphology and the microstructure of the samples were analyzed by FE-SEM (FEI Nova 400 FEG), energy dispersive X-ray spectra (EDX, OXFORD Link-ISIS-300), and XRD (XRD-6000, Shimadzu), respectively. Electrochemical measurements were conducted in a three-electrode cell system. The electrode area of the working electrode is 1 cm^2. A Pt/Ti plate in parallel orientation to the working electrode was used as the counter electrode and a saturated calomel electrode (SCE) as the reference electrode. All potentials mentioned in this work are referred to SCE. The performance of prepared electrodes toward CER and OER were examined in 5 M NaCl and 5 M $NaNO_3$, respectively.

3 Results and discussion

3.1 Surface morphology

FE-SEM analysis was performed to investigate the morphology and the effect of the microstructure of the coatings on the electrochemical performance. Figure 1 shows FE-SEM images of the support and coatings. As illustrated in Fig. 1a, the structure of the TNTs is a highly ordered and vertically oriented nanotubes, which is beneficial for the dispersion of the active species. Figure 1c, d displays the images of $(Ru_{0.3}Ti_{0.7})O_2$ and $(Ru_{0.3}Ti_{0.34}Sn_{0.3}Sb_{0.06})O_2$ deposited one time on the TNTs, respectively. The particles are both on the mouth surface and inside the nanotubes. Nevertheless, the dispersed particles of $(Ru_{0.3}Ti_{0.34}Sn_{0.3}Sb_{0.06})O_2$ are smaller than those of $(Ru_{0.3}Ti_{0.7})O_2$ on the TNTs. This is attributed to the Sn^{4+} and Sb^{3+} ions having ionic radii similar to those of Ru^{4+} and Ti^{4+}, which means they satisfy the Hume–Rothery conditions for the formation of a substitution solid solution, promoting the grain refinement and dispersion [23, 24]. For the traditional DSA, $(Ru_{0.3}Ti_{0.7})O_2$/Ti (Fig. 1b), the coating was deposited on the Ti substrate with an obvious mud-crack island-gap surface microstructure due to the thermally induced internal stresses [25]. By using the TNTs as support, however, the coating with the compact and free-crack microstructure is obtained in Fig. 1e, f. The compact oxide catalysts are composed of close-packed particles. In general, crack-free coatings can be prepared either by sol–gel deposition [12, 26, 27] or by sol–gel/electrophoretic deposition [28, 29]. In this work, we found that application of different supports also result in the different surface morphologies for the coatings. It is considered that the uninterrupted mouths of the TNTs play an important role in relieving the stress of the coating at the process of annealing. Actually, the uninterrupted mouths of the TNTs consist of numerous regular nanotubes with cylindrical structure. The accumulated stress of the coating on the TNTs support could be scattered on each nanotubes, weakening the stress concentrating on the support. Thus, the common coating with mud-cracks could be avoided using the TNTs as a support other than using sol–gel and electro-deposition methods.

3.2 Influence of Sn and Sb additives and the annealing mode

The crystalline phase of the support and coatings investigated by XRD are shown in Fig. 2a. The presence of both anatase and rutile is evident in the XRD patterns of the TNTs support. In addition to the peaks from the support, for all of the coatings, the broad and symmetric peaks at 28.72°, 35.11°, and 54.26° are attributed to diffraction peaks of RuO_2. However, the peak positions deviated slightly from the peak positions of pure RuO_2 (ICDD-JCPDDS card No. 40-1290). With respect to the $(Ru_{0.3}Ti_{0.34}Sn_{0.3}Sb_{0.06})O_2$–TNTs, the intensities of the diffraction peaks at 28.72° and 35.11°, obviously, decrease after the tin and antimony species were introduced. Although neither a SnO_2 nor a Sb_2O_5 phase was detected in the XRD patterns of the coatings, EDX analysis shows the presence of tin and antimony in the coating (Fig. 2b). And the contents of the elements in the coatings obtained from EDX analysis are summarized in Table 1. These facts reveal that the coating is still highly intermixed; i.e., the $(Ru_{0.3}Ti_{0.34}Sn_{0.3}Sb_{0.06})O_2$ film mainly exists in the form of a solid solution [30]. However, the tin content is much lower than the nominal composition. It was reported that $SnCl_4$ volatilizes easily and the tin loss could be as high as 40.0–80.0 % during the thermal decomposition process [31, 32]. Therefore, the low tin content detected by EDX is rational. In addition, compared with the diffraction peak intensity of the $(Ru_{0.3}Ti_{0.34}Sn_{0.3}Sb_{0.06})O_2$/(773 K annealed)TNTs (Fig. 2a4), the diffraction peak intensity of the anatase TiO_2 observed at $2\theta = 25.65°$ on $(Ru_{0.3}Ti_{0.34}Sn_{0.3}Sb_{0.06})O_2$–TNTs (Fig. 2a3) is comparatively weaker, whereas the intensities of the rutile phase at $2\theta = 28.72°$ and 35.11° are stronger for the TNTs support that was not subjected to an early-stage annealing pretreatment at 773 K under ambient air. The results indicate that the rutile phase of RuO_2 and SnO_2 might induce the amorphous TiO_2 to more likely crystallize the rutile rather than the anatase after the late-stage annealing at 773 K [33], which is beneficial for forming solid solutions [34, 35]. Even if the active component does not form a solid solution with the other oxides, the same rutile structure will allow for an intimate contact and a strong adhesion, thus improving the long-term durability of the coatings.

3.3 Influence of microstructure of the coatings on the active surface area

Charge or capacitance is often used to evaluate the electrochemically active surface area of an electrode. Charges of CV at different scan rates can indirectly assess the nanopore structure of an electrode infiltrated electrochemically by the electrolyte through micrometer-scale cracks. The voltammetric charge (q_a) obtained through integration of the area of the cyclic voltammogram has been used as an indicator of the accessible electrochemical activity surface area [36]. And q_a has been found to decrease as the potential sweep rate increases. For a porous electrode, at high sweep rates, only the surface that the electrolyte can penetrate is believed to take part in the charging process. In contrast, at low sweep rates, the surface that the electrolyte may not easily contact can also

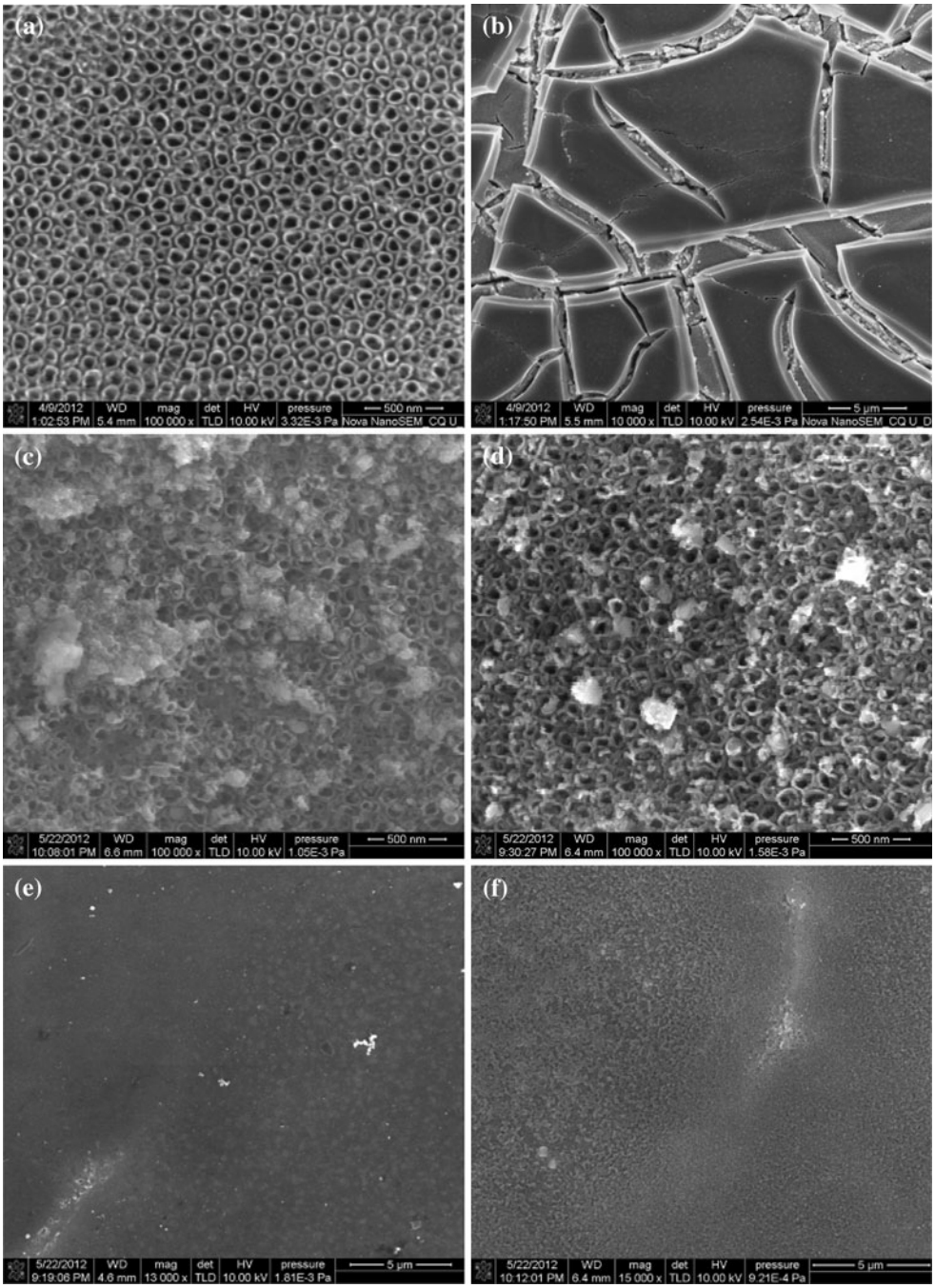

Fig. 1 FE-SEM images of samples: **a** TNTs, **b** $(Ru_{0.3}Ti_{0.7})O_2$/Ti, **c** $(Ru_{0.3}Ti_{0.7})O_2$–TNTs (deposited one time), **d** $(Ru_{0.3}Ti_{0.34}Sn_{0.3}Sb_{0.06})O_2$–TNTs (deposited one time), **e** $(Ru_{0.3}Ti_{0.7})O_2$–TNTs, and **f** $(Ru_{0.3}Ti_{0.34}Sn_{0.3}Sb_{0.06})O_2$–TNTs

participate in the charging process because sufficient time allows the electrolyte to penetrate the surface through pores, cracks, and grain boundaries in the coating. Therefore, more surface area could be utilized at lower sweep rates, resulting in a high value of q_a. Figure 3 displays the changes in q_a of these electrodes with the potential sweep rate. Obviously, the $(Ru_{0.3}Ti_{0.34}Sn_{0.3}Sb_{0.06})O_2$ supported on the TNTs has a higher q_a value; i.e., it has a greater electrochemically active surface area, compared with the traditional $(Ru_{0.3}Ti_{0.7})O_2$/Ti. Unlike a rapid decrease of q_a observed in a mud-crack coating of the $Ru_{0.3}Ti_{0.7})O_2$/Ti (Fig. 3a), $(Ru_{0.3}Ti_{0.34}Sn_{0.3}Sb_{0.06})O_2$–TNTs with a fine and uniform assembly of close-packed catalyst particles shows only a moderate decrease in q_a as the sweep rate increases, as shown in Fig. 3b–e. The result indicates that the surface nanopores packed by the particles for the $(Ru_{0.3}Ti_{0.34}$

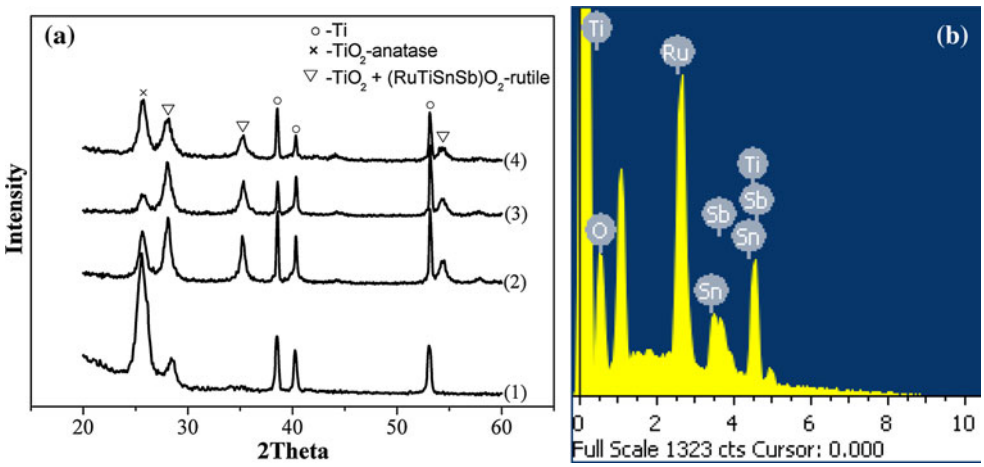

Fig. 2 **a** XRD patterns of samples: (*1*) TNTs, (*2*) $(Ru_{0.3}Ti_{0.7})O_2$–TNTs, (*3*) $(Ru_{0.3}Ti_{0.34}Sn_{0.3}Sb_{0.06})O_2$–TNTs, and (*4*) $(Ru_{0.3}Ti_{0.34}Sn_{0.3}Sb_{0.06})O_2$/(773 K annealed)TNTs, **b** EDX spectra of $(Ru_{0.3}Ti_{0.34}Sn_{0.3}Sb_{0.06})O_2$–TNTs

Table 1 EDX analysis of the coatings for the anodes

Electrodes	Atom %					
	Ru	Ti	Sn	Sb	O	Totals
$(Ru_{0.3}Ti_{0.7})O_2$/Ti	12.01	29.52	–	–	58.47	100
$(Ru_{0.3}Ti_{0.7})O_2$–TNTs	11.83	27.77	–	–	60.40	100
$(Ru_{0.3}Ti_{0.34}Sn_{0.3}Sb_{0.06})O_2$–TNTs	12.22	14.61	6.37	2.89	63.91	100

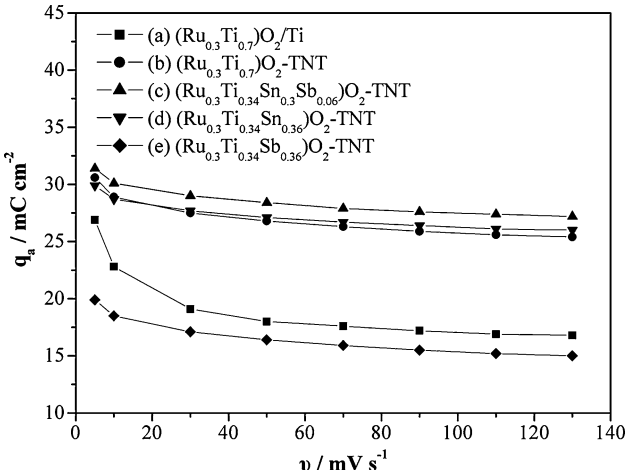

Fig. 3 Voltammetric charge (q_a) versus the potential sweep rate (υ) for the anodes

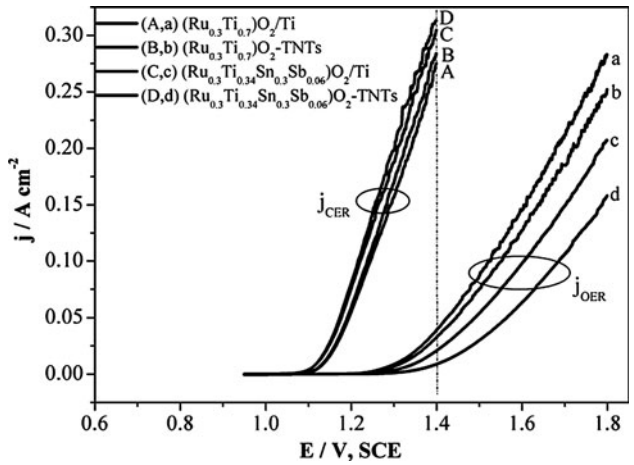

Fig. 4 LSV obtained from different anodes in 5 M NaCl and 5 M $NaNO_3$, respectively, at a sweep rate of 5 mV s^{-1}

$Sn_{0.3}Sb_{0.06})O_2$–TNTs are much more uniform and accessible by the electrolyte compared to that for the $(Ru_{0.3}Ti_{0.7})O_2$/Ti. And the compact and nano-porosity of the coating is prospective to effectively restrain the mechanical erosion caused by gas evolution and electrolyte turbulence [10, 12]. However, the $(Ru_{0.3}Ti_{0.34}Sb_{0.36})O_2$–TNTs shows the lowest q_a value among the whole anodes. The reason is that the antimony is not an active ingredient in CER, but an appropriate amount of antimony doped into the coatings plays an important role in improving the electrical conductivity and refining the grains [22, 37]. Accordingly, the relatively high antimony content for the $(Ru_{0.3}Ti_{0.34}Sb_{0.36})O_2$–TNTs might cause the structural damage of the solid solution and a remarkable decrease in the electrochemically active surface area.

3.4 Electrocatalytic activity of CER for the anodes

In general, the anodic CER reaction is accompanied by a minor OER, especially at large current densities. The

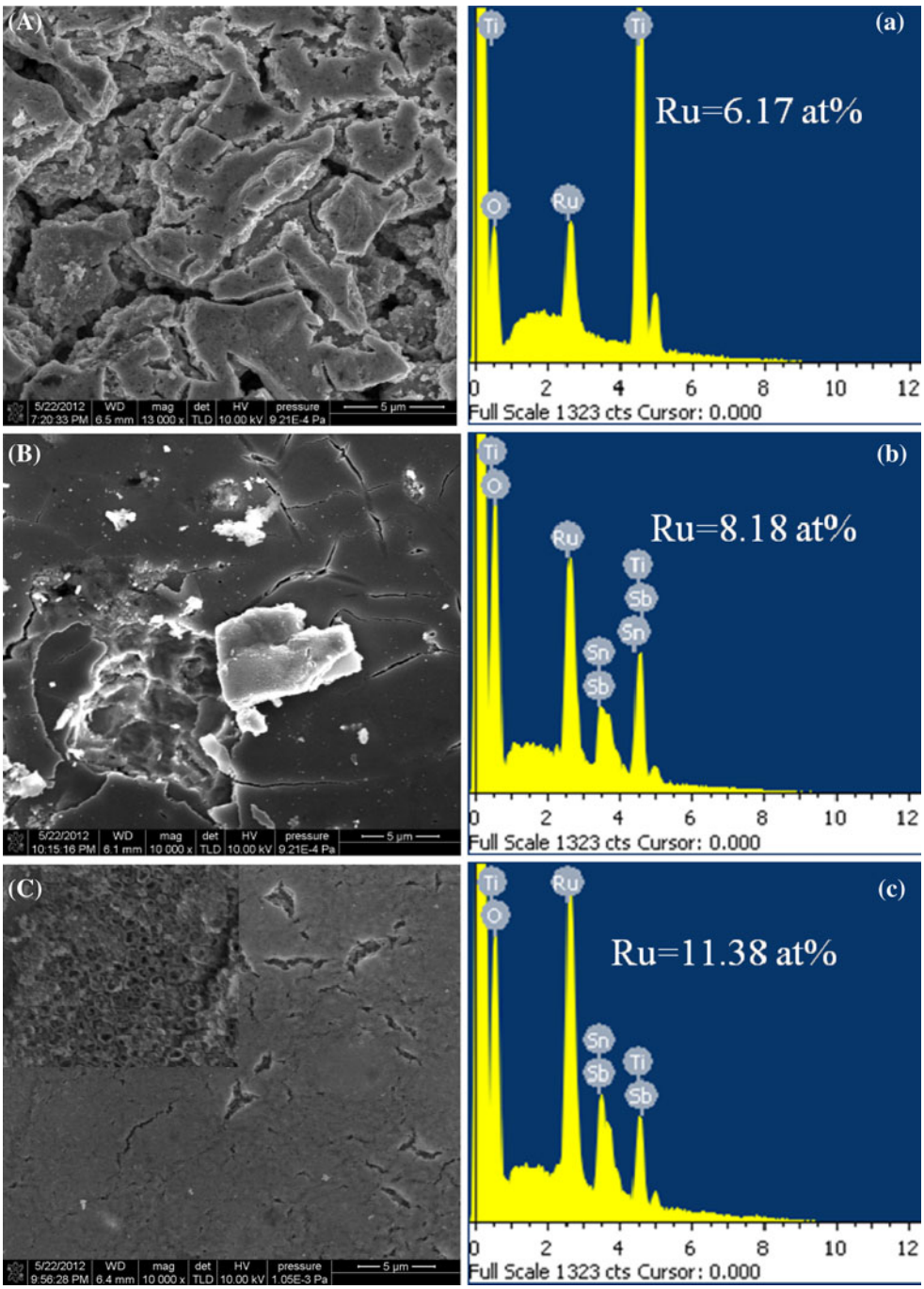

Fig. 5 FE-SEM images and corresponding EDX analysis of (**A**, **a**) used $(Ru_{0.3}Ti_{0.7})O_2$/Ti, (**B**, **b**) used $(Ru_{0.3}Ti_{0.34}Sn_{0.3}Sb_{0.06})O_2$/Ti; and (**C**, **c**) used $(Ru_{0.3}Ti_{0.34}Sn_{0.3}Sb_{0.06})O_2$–TNTs

evolution of oxygen not only contaminates the product of chlorine but also generates and thickens TiO_2 passive film between the Ti substrate and the coatings. Therefore, OER should be minimized. To simulate the performance of the electrodes for the catalysis of CER and OER, LSV was performed in 5 M NaCl and 5 M $NaNO_3$ solutions, respectively. As evidence from the results in Fig. 4, the onset potentials of CER shift slightly toward the negative direction in the order of $(Ru_{0.3}Ti_{0.34}Sn_{0.3}Sb_{0.06})O_2$–TNTs < $(Ru_{0.3}Ti_{0.34}Sn_{0.3}Sb_{0.06})O_2$/Ti < $(Ru_{0.3}Ti_{0.7})O_2$–TNTs < $(Ru_{0.3}Ti_{0.7})O_2$/Ti for CER under the identical conditions. For the onset potentials of OER, fortunately, LSV behavior indicates an obvious opposite trend to CER. The $(Ru_{0.3}Ti_{0.34}Sn_{0.3}Sb_{0.06})O_2$–TNTs without crack displays the best CER activity and the largest potential difference (ΔE) between CER and OER among the anodes studied, which is beneficial for increasing the selectivity toward CER. The reason is probably due to the facilitated diffusion and the transport of the reactive species and products through the crack-free surface, which has a

greater electrochemically active surface area. In addition, tin and antimony species co-doped into the coating effectively inhibits OER [38, 39]. These reveal that the anode without crack by utilizing the TNTs as the support could be used as an alternative for CER, which shows better activity and selectivity than the traditional $(Ru_{0.3}Ti_{0.7})O_2$/Ti. Furthermore, the compact coating could effectively resist the catalyst exfoliation caused by gas evolution and the turbulence of electrolyte.

Figure 5 shows the FE-SEM images and EDX analysis of the anodes after a period of electrolysis reaction. In the case of the used $(Ru_{0.3}Ti_{0.7})O_2$/Ti and $(Ru_{0.3}Ti_{0.34}Sn_{0.3}Sb_{0.06})O_2$/Ti anodes with mud-cracks, part of the coating peels off from the Ti substrate. At the same time, the Ru content decrease. In contrast, for the used $(Ru_{0.3}Ti_{0.34}Sn_{0.3}Sb_{0.06})O_2$–TNTs anode, the surface of the coating is still uniform and compact with a high Ru content according to the EDX results. Furthermore, the inset FE-SEM image obtained by scratching off the coating (Fig. 5c) reveals that the inner TNTs structure is preserved after the harsh electrolysis reaction. The difference in Ru content of the used $(Ru_{0.3}Ti_{0.7})O_2$/Ti and $(Ru_{0.3}Ti_{0.34}Sn_{0.3}Sb_{0.06})O_2$/Ti anodes indicates that the addition of Sn and Sb inhibits part of RuO_2 dissolution due to the formation of a solid solution of $(RuTiSnSb)O_2$. The difference in Ru content and morphology of the used $(Ru_{0.3}Ti_{0.34}Sn_{0.3}Sb_{0.06})O_2$–TNTs and $(Ru_{0.3}Ti_{0.34}Sn_{0.3}Sb_{0.06})O_2$/Ti anodes indicates that the use of TNTs can make the coating with the compact and crack-free morphology and improve the adhesion between the coating and the support. Accordingly, the compact coating cannot easily flake off from the Ti substrate and is more stable compared to that of the traditional DSA. Similar findings have been reported by Chen et al. [12] in their studies of microstructural impact of anodes on CER. They found that CER has been significantly impacted on by the surface microstructure of the coating. And the Cl_2 bubbles detached easily from the coatings with crack-free leading to a relative low surface coverage, compared to the catalysts with mud-crack. Consequently, it displays excellent electrocatalytic performance for CER during the electrolysis reaction.

4 Conclusions

The $(Ru_{0.3}Ti_{0.34}Sn_{0.3}Sb_{0.06})O_2$–TNTs anode reported herein exhibits a uniform and compact morphology without crack, which is attributed to the uninterrupted mouth of the TNTs for relieving the accumulated stress of the coating at the process of annealing. The addition of an appropriate amount of tin and antimony, not only improved the electrochemically selectivity toward CER, but also enhanced the adhesion strength between the coating and the TNTs. These improvements were attributed to the Sn^{4+} and Sb^{3+} ions having ionic radii similar to those of Ru^{4+} and Ti^{4+}, which means they satisfy the Hume–Rothery conditions for the formation of a substitution solid solution. As a result, the $(Ru_{0.3}Ti_{0.34}Sn_{0.3}Sb_{0.06})O_2$–TNTs anode exhibited superior electrocatalytic performance and excellent stability compared to those of the traditional DSA.

Acknowledgments This research work was financially sponsored by the National Basic Research Program of China (Grant Nos.: 2012CB720303 and 2012CB215501) and the National Natural Science Foundation of China (Grant Nos.: 51072239, 21176327, and 20936008).

References

1. Fauvarque J (1996) The chlorine industry. Pure Appl Chem 68:1713–1720
2. Moussallem I, Jorissen J, Kunz U, Pinnow S, Turek T (2008) Chlor-alkali electrolysis with oxygen depolarized cathodes: history, present status and future prospects. J Appl Electrochem 38:1177–1194
3. Over H (2013) Atomic scale insights into electrochemical versus gas phase oxidation of HCl over RuO_2-based catalysts: a comparative review. Electrochim Acta 93:314–333
4. Beer HB (1965) Improvements in or relating to electrodes for electrolysis. British Patent
5. Beer HB (1980) The invention and industrial-development of metal anodes. J Electrochem Soc 127:303C–307C
6. Trasatti S (1987) Progress in the understanding of the mechanism of chlorine evolution at oxide electrodes. Electrochim Acta 32:369–382
7. Trasatti S (2000) Electrocatalysis: understanding the success of DSA. Electrochim Acta 45:2377–2385
8. Rossmeisl J, Qu ZW, Zhu H, Kroes GJ, Norskov JK (2007) Electrolysis of water on oxide surfaces. J Electroanal Chem 607:83–89
9. Hansen HA, Man IC, Studt F, Abild-Pedersen F, Bligaard T, Rossmeisl J (2010) Electrochemical chlorine evolution at rutile oxide (110) surfaces. Phys Chem Chem Phys 12:283–290
10. Bommaraju TV, Chen CP, Birss VI (2001) Deactivation of thermally formed $RuO_2 + TiO_2$ coating during chlorine evolution: mechanisms and reactivation measures. Mod Chlor-Alkali Technol 8:57–81
11. Takasu Y, Sugimoto W, Nishiki Y, Nakamatsu S (2010) Structural analyses of RuO_2–TiO_2/Ti and IrO_2–RuO_2–TiO_2/Ti anodes used in industrial chlor-alkali membrane processes. J Appl Electrochem 40:1789–1795
12. Chen R, Trieu V, Zeradjanin AR, Natter H, Teschner D, Kintrup J, Bulan A, Schuhmann W, Hempelmann R (2012) Microstructural impact of anodic coating on the electrochemical chlorine evolution reaction. Phys Chem Chem Phys 14:7392–7399
13. Kota R, Stucki S (1986) Stabilization of RuO_2 by IrO_2 for anodic oxygen evolution in acid-media. Eletrochim Acta 31:1311–1316
14. Profeti D, Lassali TAF, Olivi P (2006) Preparation of $Ir_{0.3}Sn_{(0.7-x)}Ti_xO_2$ electrodes by the polymeric precursor method: characterization and lifetime study. J Appl Electrochem 36:883–888
15. Seifollahi M, Jafarzadeh K (2009) Stability and morphology of $(Ti_{0.1}Ru_{0.2}Sn_{0.7})O_2$ coating on Ti in chlorakali medium. Corros Eng Sci Technol 44:362–368
16. Sun WT, Yu Y, Pan HY, Gao XF, Chen Q, Peng LM (2008) CdS quantum dots sensitized TiO_2 nanotube-array photoelectrodes. J Am Chem Soc 130:1124–1125

17. Kuang DB, Brillet J, Chen P, Takata M, Uchida S, Miura H, Sumioka K, Zakeeruddin SM, Gratzel M (2008) Application of highly ordered TiO_2 nanotube arrays in flexible dye-sensitized solar cells. ACS Nano 2:1113–1116
18. Kim JH, Zhu K, Yan YF, Perkins CL, Frank AJ (2010) Microstructure and pseudocapacitive properties of electrodes constructed of oriented NiO–TiO_2 nanotube arrays. Nano Lett 10: 4099–4104
19. Ortiz GF, Hanzu L, Djenizian T, Lavela P, Tirado JL, Knauth P (2009) Alternative Li-ion battery electrode based on self-organized titania nanotubes. Chem Mater 21:63–67
20. Pan K, Tian M, Jiang ZH, Kjartanson B, Chen AC (2012) Electrochemical oxidation of lignin at lead dioxide nanoparticles photoelectrodeposited on TiO_2 nanotube arrays. Electrochim Acta 60:147–153
21. Wang YQ, Wei ZD, Gao B, Qi XQ, Li L, Zhang Q, Xia MR (2011) The electrochemical oxidation of methanol on a Pt/TNTs/Ti electrode enhanced by illumination. J Power Sources 196: 1132–1135
22. Cao HZ, Lu DH, Lin JP, Ye Q, Wu JJ, Zheng GQ (2013) Novel Sb-doped ruthenium oxide electrode with ordered nanotube structure and its electrocatalytic activity toward chlorine evolution. Electrochim Acta 91:234–239
23. Gaudet J, Tavares AC, Trasatti S, Guay D (2005) Physicochemical characterization of mixed RuO_2–SnO_2 solid solutions. Chem Mater 17:1570–1579
24. Kong HS, Lu HY, Zhang WL, Lin HB, Huang WM (2012) Performance characterization of Ti substrate lead dioxide electrode with different solid solution interlayers. J Mater Sci 47: 6709–6715
25. Trasatti S (1994) The electrochemistry of novel materials. Frontiers of electrochemistry. VCH Publishers, Weinheim, pp 207–295
26. Macounova K, Makarova M, Jirkovsky J, Franc J, Krtil P (2008) Parallel oxygen and chlorine evolution on $Ru_{1-x}Ni_xO_{2-y}$ nanostructured electrodes. Electrochim Acta 53:6126–6134
27. Forti JC, Olivi P, de Andrade AR (2001) Characterisation of DSA-type coatings with nominal composition $Ti/Ru_{0.3}Ti_{(0.7-x)}Sn_xO_2$ prepared via a polymeric precursor. Electrochim Acta 47:913–920
28. Zhitomirsky I (2002) Cathodic electrodeposition of ceramic and organoceramic materials. Fundamental aspects. Adv Colloid Interface Sci 97:279–317
29. Yousefpour M, Shokuhy A (2012) Electrodeposition of TiO_2–RuO_2–IrO_2 coating on titanium substrate. Superlattice Microstruct 51:842–853
30. Chen SY, Zheng YH, Wang SW, Chen XM (2011) Ti/RuO_2–Sb_2O_5–SnO_2 electrodes for chlorine evolution from seawater. Chem Eng J 172:47–51
31. Comninellis C, Vercesi GP (1991) Problems in DSA coating deposition by thermal decomposition. J Appl Electrochem 21: 136–142
32. Lassali TAF, Bulhoes OS, Abeid LMC, Boodts JFC (1997) Surface characterization of thermally prepared, Ti-supported, Ir-based electrocatalysts containing Ti and Sn. J Electrochem Soc 144:3348–3354
33. Chang SY, Chen SF, Huang YC (2011) Synthesis, structural correlations, and photocatalytic properties of TiO_2 nanotube/SnO_2–Pd nanoparticle heterostructures. J Phys Chem C 115: 1600–1607
34. Roginskaya YE, Bystrov VI, Shub DM (1977) X-ray-diffraction and micro X-ray spectral study of RuO_2–TiO_2–Cl system. Zh Neorg Khim 22:201–205
35. Jacob KT, Subramanian J (2008) Phase diagram for the system RuO_2–TiO_2 in air. J Phase Equilib Diffus 29:136–140
36. Doubova LM, Daolio S, DeBattisti A (2002) Examination of RuO_2 single-crystal surface: charge storage mechanism in H_2SO_4 aqueous solution. J Electroanal Chem 532:25–33
37. Lee KS, Park IS, Cho YH, Jung DS, Jung N, Park HY, Sung YE (2008) Electrocatalytic activity and stability of Pt supported on Sb-doped SnO_2 nanoparticles for direct alcohol fuel cells. J Catal 258:143–152
38. Kotz R, Stucki S, Carcer B (1991) Electrochemical waste water treatment using high overvoltage anodes. Part I: physical and electrochemical properties of SnO_2 anodes. J Appl Electrochem 21:14–20
39. Chen AC, Nigro S (2003) Influence of a nanoscale gold thin layer on Ti/SnO_2–Sb_2O_5 electrodes. J Phys Chem B 107:13341–13348